Zygotically controlled F-actin establishes cortical compartments to stabilize furrows during *Drosophila* cellularization

Anna Marie Sokac[1] and Eric Wieschaus[1,2,*]

[1]Department of Molecular Biology and [2]Howard Hughes Medical Institute, Princeton University, Washington Road, Princeton, NJ 08544, USA
*Author for correspondence (e-mail: efw@princeton.edu)

Summary

Cortical compartments partition proteins and membrane at the cell surface to define regions of specialized function. Here we ask how cortical compartments arise along the plasma membrane furrows that cellularize the early *Drosophila* embryo, and investigate the influence that this compartmentalization has on furrow ingression. We find that the zygotic gene product Nullo aids the establishment of discrete cortical compartments, called furrow canals, which form at the tip of incipient furrows. Upon *nullo* loss-of-function, proteins that are normally restricted to adjacent lateral regions of the furrow, such as Neurotactin and Discs large, spread into the furrow canals. At the same time, cortical components that should concentrate in furrow canals, such as Myosin 2 (Zipper) and Anillin (Scraps), are missing from some furrows. Depletion of these cortical components from the furrow canal compartments precipitates furrow regression. Contrary to previous models, we find that furrow compartmentalization does not require cell-cell junctions that border the furrow canals. Instead, compartmentalization is disrupted by treatments that reduce levels of cortical F-actin. Because the earliest uniform phenotype detected in *nullo* mutants is reduced levels of F-actin at furrow canals, we propose that Nullo compartmentalizes furrows via its regulation of F-actin, thus stabilizing furrows and insuring their ingression to complete cellularization.

Supplementary material available online at
http://jcs.biologists.org/cgi/content/full/121/11/1815/DC1

Key words: Cellularization, Cortical compartments, F-actin

Introduction

Cortical compartments partition cell surfaces into regions of specific function. Within these compartments the composition of the plasma membrane (PM), membrane-associated proteins and the underlying cortex is distinct from that of adjacent areas. During cytokinesis in budding yeast, compartments are defined by split Septin rings that form diffusion barriers on both sides of the F-actin/Myosin 2 contractile array to ensure cell scission (Dobbelaere and Barral, 2004). Alternatively, in neurons a compartment called the initial segment is established as a dense meshwork of F-actin, Ankyrin G and Spectrin that concentrates in the cortex and binds ion channels and transmembrane proteins in the PM to restrict diffusion between the axon and cell body (Dzhashiashvili et al., 2007; Nakada et al., 2003; Winckler et al., 1999). Thus, cortical compartments are generated by at least two general mechanisms: either barriers are set up at the borders of the compartment, or a dense cortical cage assembles just under the compartment itself.

Drosophila cellularization is a dramatic morphogenetic event in which PM furrows ingress between each of ~6000 cortically anchored nuclei to convert the early syncytial embryo into the cellular blastoderm (Mazumdar and Mazumdar, 2002). Discrete compartments arise along cellularization furrows as they ingress, and are first revealed by the partitioning of proteins, including F-actin and Myosin 2 (Zipper) into furrow canals that form at the tips of the incipient furrows (Warn et al., 1980; Warn and Magrath, 1983). Furrow canal compartments then lead furrow ingression to complete cellularization. It is not currently known how furrow canal compartments are established and maintained coincident with the PM growth that drives cellularization, although several possible cellular mechanisms have now been suggested. Rho-GTPase-dependent F-actin polymerization contributes to furrow canal assembly (Grosshans et al., 2005; Padash Barmchi et al., 2005), and scaffolding proteins, such as Spectrin (Pesacreta et al., 1989; Thomas and Williams, 1999) and Anillin (Scraps) (Field, S. et al., 2005), accumulate at furrow canals. This dense underlying cortical matrix is likely to define the particular molecular interactions, signaling events and membrane dynamics that can occur within the furrow canal. Also, at the beginning of cellularization, E-cadherin/Catenin-based cell-cell junctions, called basal junctions, assemble immediately apical to the furrow canals (Hunter and Wieschaus, 2000; Muller and Wieschaus, 1996). These basal junctions travel in register with the furrow canals as the furrows ingress, dynamically marking the boundary between the growing PM and furrow canal. Thus, basal junctions are positioned to block lateral diffusion between adjacent PM regions, and so may maintain furrow canal composition throughout cellularization (Lecuit and Wieschaus, 2000). Lastly, the exocytosis that feeds PM growth during cellularization (Albertson et al., 2005) is targeted to the lateral PM rather than to the furrow canal (Lecuit and Wieschaus, 2000), offering an obvious means to localize membrane growth and protect furrow canal components from dilution by new membrane insertion. Although these mechanisms offer possible ways to establish and maintain furrow canal compartments, it is not clear what role each plays, or how they are regulated or coordinated with membrane growth to sustain furrow ingression.

Zygotic transcription starts just prior to cellularization, and as such is thought to provide regulators of the maternal cellular machinery that trigger specific patterning, cell cycle and morphogenetic events (Wieschaus, 1996). A strong candidate as a zygotic regulator of cellularization is the *nullo* gene. Its transcription is purely zygotic (De Renzis et al., 2007; Rose and Wieschaus, 1992), and Nullo protein levels peak at the beginning of cellularization and then steeply decline as cellularization proceeds (Postner and Wieschaus, 1994; Rose and Wieschaus, 1992), suggesting an early role in the process. Nullo initially colocalizes with F-actin and Myosin 2 in the newly assembled furrow canals and then resolves from the furrow canals into the basal junction regions (Hunter and Wieschaus, 2000; Postner and Wieschaus, 1994), putting it in position to establish and/or maintain furrow canal compartments. *nullo* loss-of-function embryos show both basal junction and furrow canal defects (Hunter and Wieschaus, 2000; Postner and Wieschaus, 1994; Wieschaus and Sweeton, 1988), as might be predicted if basal junctions are required to establish and maintain the furrow canals. Thus, in an effort to better understand the mechanisms that partition proteins into furrow canal compartments during cellularization, and to learn how such partitioning influences furrow ingression, we focused on the relationship between furrow canal compartments and furrow dynamics in *nullo* mutant embryos.

In the experiments described below, we use various lateral membrane and furrow canal markers to follow the establishment and maintenance of cortical compartments from the beginning of cellularization. Our data suggest that Nullo is required to establish furrow canal compartments and that it does so independently of its effects on the basal junctions or the cortical scaffold protein Anillin. Instead, Nullo might establish compartments via its regulation of F-actin within the furrow. Maintenance of Myosin 2 and cortical components at the furrow canal compartments stabilizes furrows and ensures their ingression. These findings refute a widely held model that cell-cell junctions are required for furrow ingression during *Drosophila* cellularization. Rather, we propose that it is the dense matrix of cortical F-actin that sustains ingression to complete cellularization.
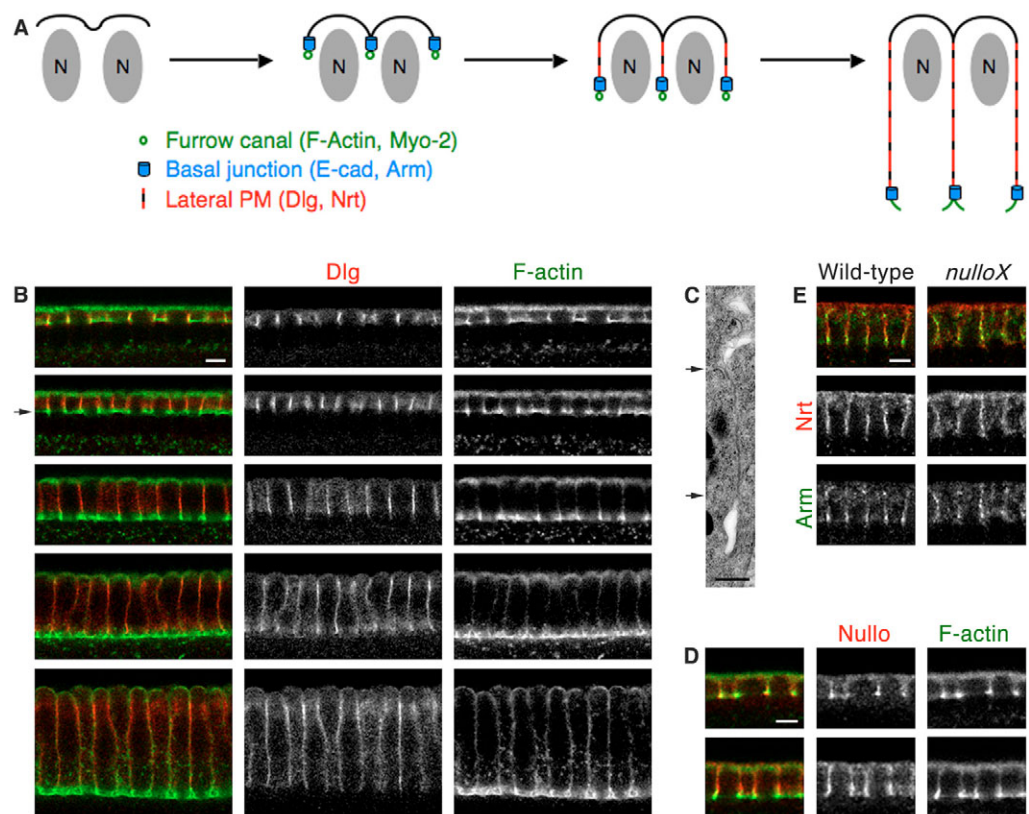
Results

Nullo contributes to furrow compartmentalization

At mitotic cycle 14, the embryo pauses in a prolonged interphase and cortical domes called somatic buds form over each nucleus (Schejter and Wieschaus, 1993). Cellularization starts at the sites where bud margins meet and ingress as furrows (Fig. 1A). F-actin and Myosin 2 assemble into furrow canals at these incipient furrow tips, and junctional components coalesce in adjacent basal junctions. Furrow canals then lead furrow ingression to cellularize the embryo. We followed protein dynamics at the onset of cellularization to see when cortical compartments are clearly distinguishable along the furrow length. At the beginning of cellularization, the PDZ-containing scaffold protein Discs large (Dlg) is spread along the juxtaposed bud margins and colocalizes with lateral F-actin (Fig. 1B). However, these markers separate as bud margins transition into obvious furrows. This

Fig. 1. Furrow canals are established as discrete cortical compartments at the onset of cellularization. (A) Illustration showing somatic buds over each nucleus (N) extending their margins to form cellularization furrows. At early cellularization, F-actin and Myosin 2 (Myo-2) furrow canals assemble at the furrow tips and E-cadherin (E-cad) and β-catenin (Arm) coalesce into adjacent basal junctions. Basal junctions mark the boundary between furrow canal compartments and the growing lateral plasma membrane (PM). Furrow canals and basal junctions travel in register at the tip of the ingressing furrow until late cellularization, when furrow canals contract to close off the basal ends of the cells. (B,D,E) Confocal images of cellularizing embryos. (B) Cross-sections showing overlap between the PM component Dlg (red) and F-actin (green) as furrows first form. These markers are resolved once furrows reach a length of 5 μm (arrow in B) with Dlg restricted to the lateral PM and F-actin concentrating in the furrow canals. This compartmentalization is maintained throughout late cellularization. (C) TEM image of an early cellularization furrow with arrows indicating the apical (top) and basal (bottom) boundary of the lateral PM. The furrow canal compartment appears as a broadening at the furrow tip. (D) Cross-sections showing Nullo first concentrating with F-actin in early furrow canals and then concentrating at the basal junction regions slightly later. (E) Cross-sections showing Arm accumulating in basal junctions at the basal-most region of the lateral PM (Nrt, red) in wild-type embryos as compared with spreading along the PM in *nulloX* embryos. Scale bars: 5 μm in B,D,E and 500 nm in C.

takes ~5-8 minutes and, in the resulting furrows of 5 µm length, Dlg is restricted to the lateral PM, whereas F-actin clearly concentrates in the furrow canal. This asymmetric distribution of Dlg and F-actin then persists through later cellularization (Lee et al., 2003). Thus, cortical components partition into discrete compartments at a furrow length of 5 µm and this distribution is maintained throughout cellularization, coinciding in space and time with the establishment and maintenance of PM compartments (Lecuit and Wieschaus, 2000). By transmission electron microscopy (TEM), furrow canal compartments are morphologically distinct from the lateral PM in furrows measuring >5 µm in length, appearing as broadenings at the furrow tip (Fig. 1C).

How compartments arise along the cellularization furrows is not clear. *nullo* loss-of-function (*nulloX*) embryos display both furrow canal and basal junction defects (Fig. 1E) (Hunter and Wieschaus, 2000), as is predicted if basal junctions establish and/or maintain furrow canal compartments. At the beginning of cellularization, zygotically expressed Nullo concentrates with F-actin and Myosin 2 in assembling furrow canals and then resolves from the furrow canals into the basal junction regions (Fig. 1D) (Hunter and Wieschaus, 2000; Postner and Wieschaus, 1994). In *nulloX* embryos, basal junction components are spread along the furrows rather than coalescing into distinct basal junctions (Hunter and Wieschaus, 2000; Postner and Wieschaus, 1994; Wieschaus and Sweeton, 1988). In addition, both F-actin and Myosin 2 are missing from a fraction of furrow canal compartments, such that breaks appear in the furrow canal network (Hunter and Wieschaus, 2000; Postner and Wieschaus, 1994; Wieschaus and Sweeton, 1988). We wondered whether these previously described *nulloX* phenotypes correlate with compromised furrow compartmentalization.

We imaged markers that are normally restricted to the lateral PM of the cellularization furrows, and found that Dlg staining spreads into the furrow canal compartments of *nulloX* embryos throughout cellularization. Dlg is detected in furrow canals even at the earliest stages of cellularization when furrows have reached ~5 µm (Fig. 2A), suggesting that distinct compartments might never be established in these mutants. In addition to Dlg, the transmembrane protein Neurotactin (Nrt), which adds to the growing lateral PM at mid- to late cellularization and is restricted to this location in wild-type embryos (Lecuit and Wieschaus, 2000), is seen in all furrow canals in *nulloX* embryos (Fig. 2B). Thus, furrow canal compartmentalization is compromised in *nulloX* mutants. We noted that furrow canals are abnormally flat in *nulloX* mutants (Fig. 2A,B), as compared with their normal tear-shaped morphology in wild-type embryos (Fig. 1C). TEM analysis revealed that the furrow canal broadenings at the tips of some *nulloX* furrows had collapsed (Fig. 2C), whereas others appeared abnormally flat on their basal surface with significant membrane blebbing (Fig. 2D). According to these assays, every furrow canal compartment is compromised in *nulloX* embryos. This is in contrast to furrow canal breaks, which only affect a fraction of *nulloX* furrows. Given that every furrow canal compartment contains ectopic lateral PM components and shows altered morphology in these mutants, Nullo may directly contribute to either the establishment and/or maintenance of furrow compartmentalization.

Cortical components within the furrow canal compartments ensure sustained furrow ingression

We next asked how compromised furrow canal compartments influence furrow ingression. Despite the spreading of lateral components into all furrow canal compartments in *nulloX* embryos, these furrows still ingress as cellularization proceeds in these mutants. But breaks appear in the F-actin/Myosin 2 furrow canal network, indicating the absence of cortical components from some
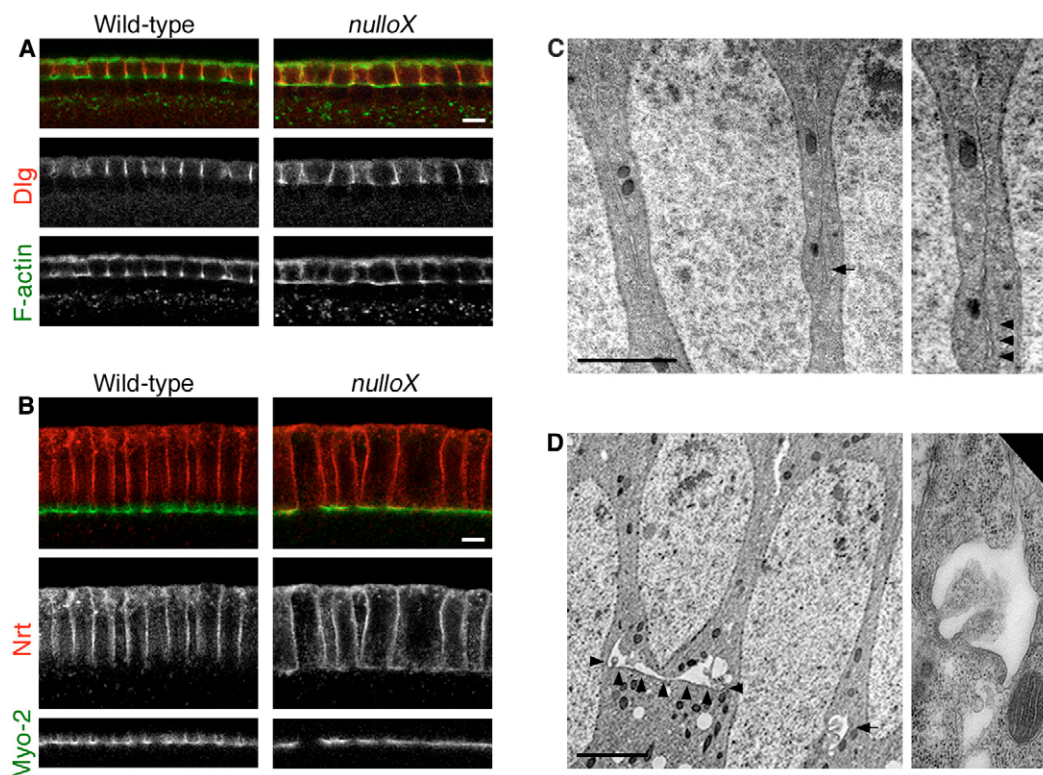
Fig. 2. Furrow canal compartments are compromised in *nulloX* embryos. (A,B) Confocal images of cellularizing embryos. (A) Cross-sections showing tear-shaped F-actin furrow canals (green) that lack Dlg staining (red) in wild-type embryos as compared with flattened furrow canals with significant Dlg staining in *nulloX* embryos. (B) Cross-sections showing tear-shaped Myosin 2 furrow canals (Myo-2, green) that lack Nrt staining (red) in wild-type embryos as compared with flattened furrow canals with significant Nrt staining in *nulloX* embryos. (C,D) TEM images showing furrows ingressing in cellularizing *nulloX* embryos. Arrows indicate the position of furrow canal, shown at higher magnification in the right-hand images. (C) Furrow canal broadenings are often collapsed at the furrow tip (arrowheads in the higher-magnification image). (D) Alternatively, furrow canals may contain PM blebs and show accentuated basal flattening (arrowheads). Scale bars: 5 µm in A,B and 2 µm in C,D.

furrow canal compartments. It has been assumed that these breaks represent sites where furrows fail to ingress, but this has not been tested. To relate furrow canal breaks with furrow dynamics we imaged Myosin 2 and the PM probe Nrt in fixed *nulloX* embryos, using furrow length as a measure of cellularization progression. In both cross-sections and single-plane images collected at the level of the furrow canals (Fig. 3A,B,D), it was clear that some breaks in the furrow canal network were due to the absence of membrane

furrows. In other cases, we surprisingly found that furrows persisted but had no Myosin 2 in the furrow canal compartment. We scored the frequency of each disrupted furrow type over the course of early to mid-cellularization (Fig. 3C; 800-1200 furrows scored from 4-6 embryos per data point). At early cellularization there were more cases of 'furrows with no Myosin 2' than of 'furrows missing'. As cellularization approached the fast phase of furrow ingression at 10-15 μm furrow length (Lecuit and Wieschaus, 2000), this
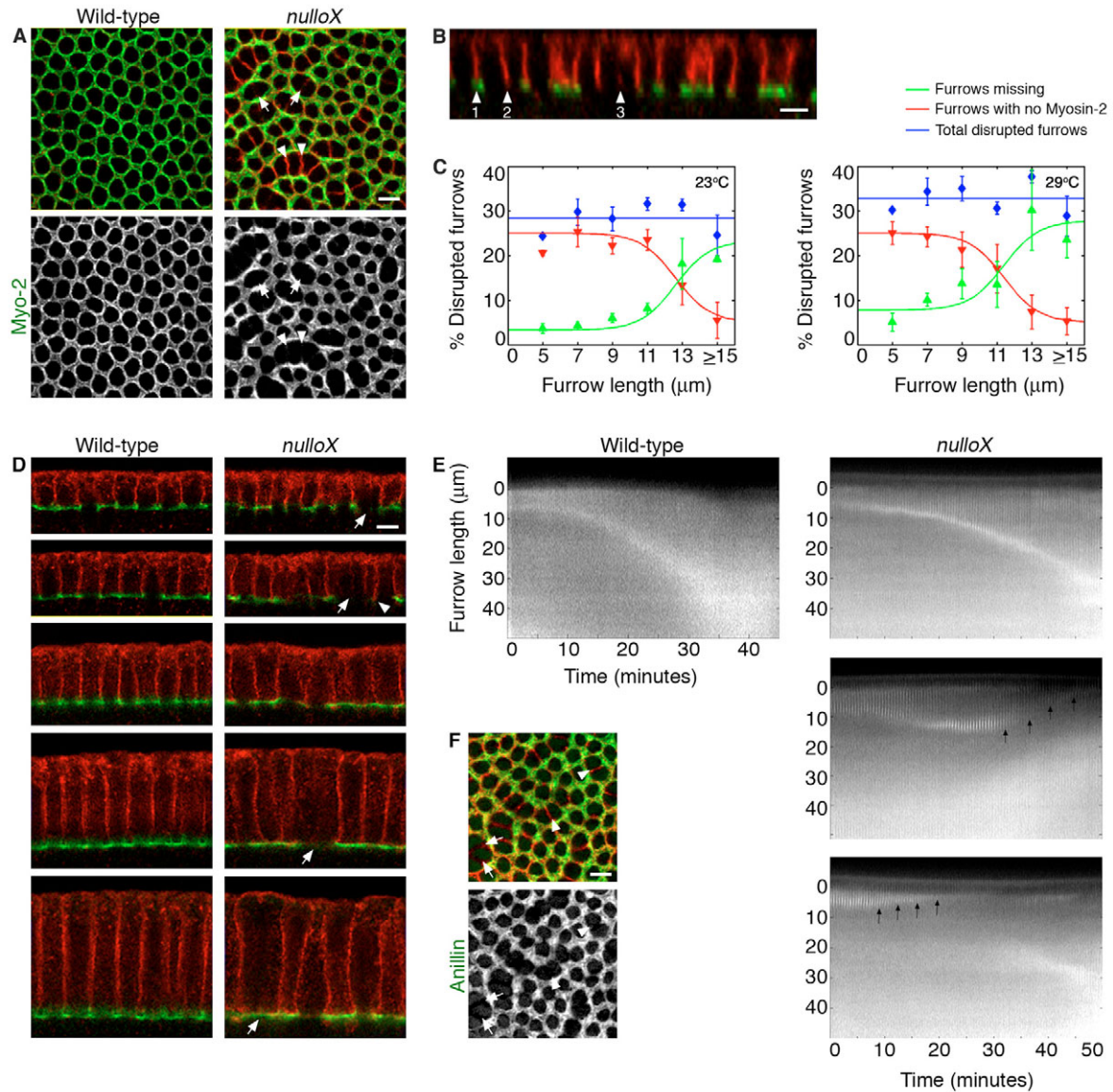
Fig. 3. The absence of Myosin 2 from furrow canals precipitates furrow regression in *nulloX* embryos. (A,B,D) Confocal images of PM furrows (Nrt, red) and Myosin 2 furrow canals (Myo-2, green) ingressing between adjacent nuclei in cellularizing embryos. (A) En face images from a single plane at the level of the furrow canals showing that in *nulloX* embryos, some furrows are missing (arrows) or have no Myosin 2 in the furrow canals (arrowheads). (B) Projected *z*-section from a *nulloX* embryo showing adjacent nuclei separated by: (1) a furrow with Myosin 2; (2) a furrow with no Myosin 2; or (3) a missing furrow. (C) The average percentage of disrupted furrows at progressive stages of cellularization in *nulloX* embryos grown at 23°C or 29°C (total disrupted furrows, blue; furrows with no Myosin 2, red; furrows missing, green). Each point represents 4-6 cellularizing embryos of the given furrow length, with ~200 interfaces scored per embryo. Error bars represent s.d. (D) Cross-sections at progressive phases of cellularization showing furrows with Myosin 2 between all nuclei in wild-type embryos. In *nulloX* embryos, some furrows are missing (arrows) or have no Myosin 2 in the furrow canals (arrowhead). (E) Kymographs showing furrow dynamics (GFP-Spider) in live cellularizing embryos (taken from supplementary material Movies 1 and 2). Three types of furrow dynamics are seen in *nulloX* embryos: (1) furrows that ingressed ~40 μm at rates comparable to those of the wild type; (2) furrows that ingressed to lengths >5 μm then regressed; and (3) furrows that ingressed to a length of only ~5 μm then regressed. Arrows follow the tip of the regressing furrows. (F) En face confocal image from a single plane at the level of the furrow canals showing PM furrows (Nrt, red) and Anillin furrow canals (green) in cellularizing *nulloX* embryos. Some furrows are missing (arrows) or have no Anillin in the furrow canals (arrowheads). Scale bars: 5 μm in A,B,D,F.

relationship was reversed. This suggests that the furrows with no Myosin 2 in the furrow canals must have ingressed for some time but then regressed because the total number of disrupted furrows did not increase. We found that the length of neighboring furrows with and without Myosin 2 in the furrow canals did not vary significantly (ratio=0.97±0.09; n=263 furrows with no Myosin 2, from 17 embryos with furrow lengths of 5-15 μm). Thus, furrows with no Myosin 2 in the furrow canal compartment can ingress for some distance, but appear to be unstable and are likely to regress over the course of cellularization.

We confirmed that these furrow dynamics are representative of events in living *nulloX* mutants using embryos that express a GFP-tagged PM probe (Gilgamesh, referred to as GFP-Spider) in a *nulloX* background. Confocal time-lapse images were collected at the embryo mid-section to capture cross-sections of the ingressing furrows (supplementary material Movies 1 and 2). Kymographs (time versus furrow length) were then generated to follow furrow dynamics (Fig. 3E). At the onset of cellularization, short, 5 μm-long furrows formed between all nuclei. After a brief pause, a small fraction of these incipient furrows immediately regressed; these probably represent those furrows from the fixed-tissue data that are missing from the beginning of cellularization. Among the remaining furrows that continued to ingress, most reached the full length of 40 μm at rates comparable to those of the wild type. However, others regressed throughout the process, appearing to snap back towards the embryo surface; these are likely to represent those furrows from the fixed-tissue data that lack Myosin 2 and regress at intermediate stages of cellularization. Thus, furrow kinetics in living *nulloX* embryos are consistent with those inferred from fixed-tissue data.

Taken together, these results demonstrate two striking relationships between furrow compartmentalization and furrow ingression. First, given that the number of furrow canals with no Myosin 2 does not increase over time, Nullo must act during compartment establishment. This is supported by the expression profile of Nullo, which peaks at the beginning of cellularization (Rose and Wieschaus, 1992). Failures in compartment establishment do not necessarily prevent furrow ingression, but correlate with later furrow regression. Second, because some furrows ingress with no Myosin 2 in the furrow canal compartment, Myosin 2 is not absolutely required within a given furrow canal in order to drive ingression of that furrow (Dawes-Hoang et al., 2005; Royou et al., 2004; Thomas and Wieschaus, 2004). Rather, Myosin 2 in furrow canal compartments stabilizes the associated furrow and so sustains ingression. We also saw that additional cortical scaffolds, including Anillin and Septin (Peanut), exhibit dynamics resembling Myosin 2 in *nulloX* embryos (Fig. 3F; data not shown), suggesting that a number of cortical components must partition into the furrow canal compartment to stabilize but not drive furrow ingression. Conversely, furrows with no detectable F-actin in the furrow canal are almost never seen in *nulloX* embryos (<0.5% furrows persist with no F-actin furrow canal; n=1831 furrows from 20 embryos with furrow lengths of 5-15 μm). Thus, it appears that when furrow canals lack sufficient cortical components, F-actin can be depleted from the compartment and this precipitates immediate furrow regression.

Basal junctions do not establish or maintain furrow canal compartments

As shown by the localization of junctional components, *nulloX* mutants display disrupted basal junctions along all cellularization furrows (Fig. 1E) (Hunter and Wieschaus, 2000). This defect correlates with breaks in the F-actin/Myosin 2 furrow canal network as is predicted if basal junctions establish and/or maintain furrow canal compartments. To then determine whether disruption of basal junctions in *nulloX* embryos can account for the compromised furrow compartmentalization or absence of cortical components from furrow canals, we eliminated basal junctions by preparing embryos that are both maternally and zygotically deficient for *armadillo* (*arm*) and scored for furrow canal defects. *arm* encodes the *Drosophila* homolog of β-catenin (Peifer and Wieschaus, 1990) and is a known component of basal junctions (Hunter and Wieschaus, 2000; Muller and Wieschaus, 1996). In single-plane confocal images of cellularizing embryos, no Arm or E-cadherin (Shotgun) was detected in *arm*[043A01] embryos at the position where basal junctions should form, in contrast to wild-type embryos that have thick plaques of Arm and E-cadherin at the basal junctions (Fig. 4A; data not shown). Cross-sections confirmed that Arm and E-cadherin were completely absent from the lateral PM in cellularizing *arm*[043A01] embryos (Fig. 4B,C; data not shown). TEM of furrows showed tight apposition between adjacent PMs in wild-type embryos, as compared with gaps in *arm*[043A01] embryos (Fig. 4D,E). Some gaps were ≥50 nm, which exceeds the distance spanned by trans-cadherin-mediated adhesion (Shapiro et al., 1995). So, as reported for other *arm* alleles (Cox et al., 1996; Harris and Peifer, 2004; Muller and Wieschaus, 1996), cell-cell adhesion is severely compromised in *arm*[043A01] embryos, and no detectable basal junctions form.

Previous data indicate that *arm*-deficient embryos can cellularize (Grevengoed et al., 2003; Cox et al., 1996), but a full analysis of furrow canal morphology has not been reported. We examined furrow canals in *arm*[043A01] embryos, looking for phenotypes that resemble the compartmentalization defects in *nulloX* mutants. We confirmed that despite the loss of basal junctions, furrows formed and ingressed around all nuclei in *arm*[043A01] embryos. Myosin 2 is maintained in a normal pattern in all furrow canals (Fig. 4F,G), and these furrow canals contracted during late cellularization when the basal surface of the cells is normally closed-off from the yolk mass (Fig. 4F). Cross-sections further revealed that *arm*[043A01] furrow canals are discrete tear-shaped compartments (Fig. 4G), and TEM confirmed that furrow tips broaden to form distinct furrow canal structures in these embryos (Fig. 4E). The characteristic accumulation of Nrt was observed in the growing lateral PM of *arm*[043A01] embryos, and did not enter the furrow canals despite the absence of intervening basal junctions (Fig. 4G). Lastly, F-actin levels in furrow canals of *arm*[043A01] embryos did not differ significantly from those of wild-type embryos (Fig. 4H,I; n=3 independent experiments), suggesting that F-actin assembly and accumulation in furrow canals does not require basal junctions. Our inability to detect furrow defects in *arm*[043A01] mutants argues that disrupted basal junctions are not responsible for the compromised furrow compartmentalization seen in *nulloX* embryos.

F-actin maintains furrow canal compartments

Since basal junctions are dispensable for establishing and maintaining furrow canal compartments, Nullo activity must compartmentalize the furrow by some alternative mechanism. In mammalian neurons, a PM compartment called the initial segment is established between the cell body and proximal region of the axon (Winckler and Mellman, 1999). Within the initial segment the lateral diffusion of lipids and proteins is limited, serving to both define a specialized compartment of the cell and to restrain the exchange of PM components between the cell body and axon. This compartment is

defined by the cortical scaffold Ankyrin G, which indirectly tethers the PM to the underlying F-actin/Spectrin meshwork (Dzhashiashvili et al., 2007; Nakada et al., 2003; Winckler et al., 1999). In *nulloX* embryos, cortical scaffold proteins such as Anilllin and Septin, which can similarly link F-actin to the PM (Field and Alberts, 1995; Field, C. et al., 2005), are depleted from some furrow canals. We therefore asked whether mislocalization of these scaffolds contributes to the loss of furrow canal compartments in *nulloX* mutants.

Severe maternal-effect alleles of Anillin (*anillin*[HP], *anillin*[RS] and *anillin*[PQ]) reduce the rate of furrow ingression during cellularization and induce furrow regression late in the process (Field, C. et al., 2005). Furthermore, Septin fails to localize to furrow canals in these mutants (Fig. 5A) (Field, C. et al., 2005). We examined furrow compartmentalization in embryos derived from transheterozygous *anillin*-deficient mothers (*anillin*[HP/RS] or *anillin*[PQ/RS]). We found that despite the loss of Anillin and Septin, Nullo concentrates at these
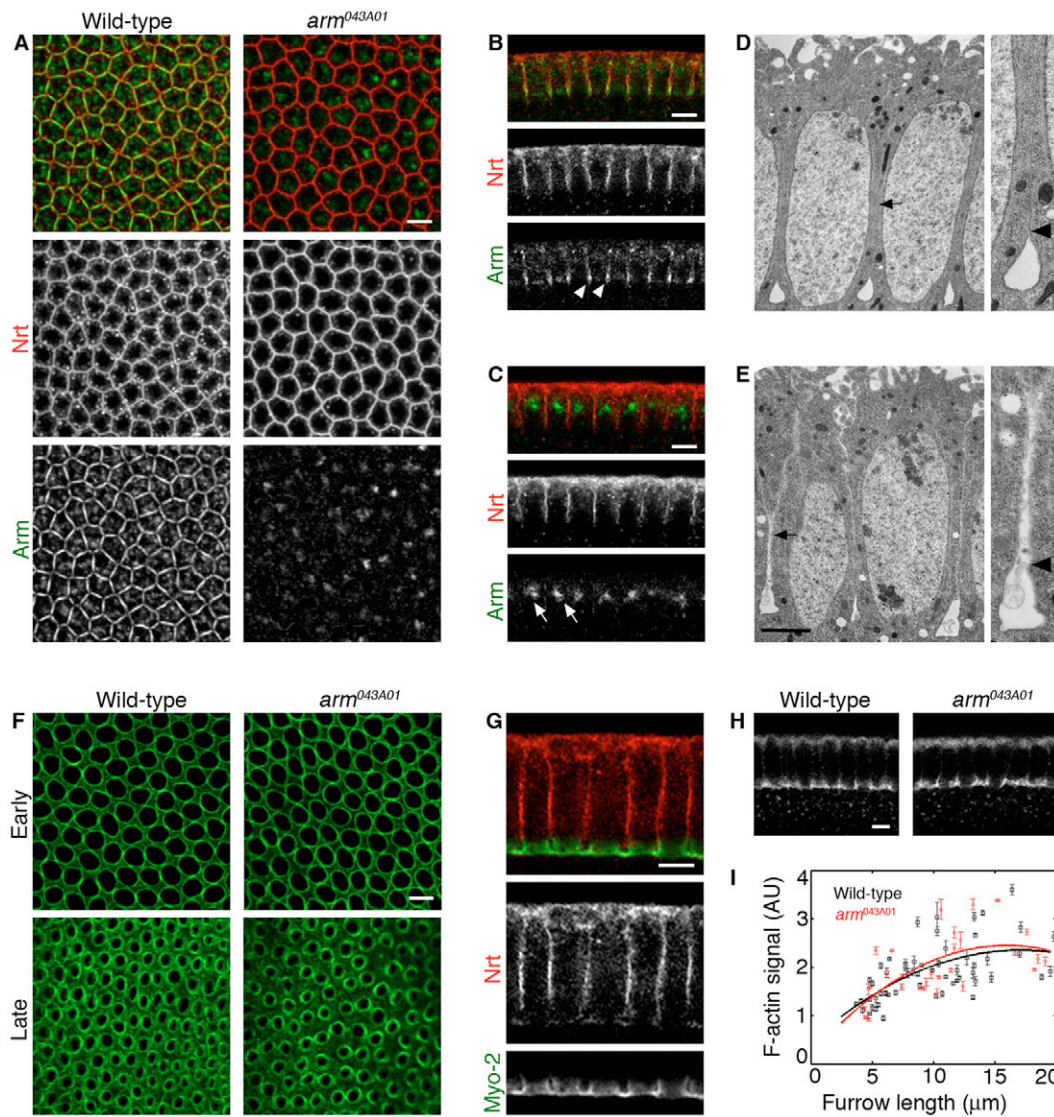
Fig. 4. Basal junctions do not assemble in *arm*[043A01] embryos, but functional furrow canal compartments are established and maintained. (A-C) Confocal images of PM (Nrt, red) and basal junctions (Arm, green) in cellularizing embryos. (A) En face images from a single plane at the level where basal junctions should be, showing that truncated Arm fails to accumulate in basal junctions in *arm*[043A01] mutants. (B) Cross-sections of a wild-type embryo showing furrows ingressing between all nuclei and Arm accumulating at basal junctions (arrowheads). (C) Cross-sections of an *arm*[043A01] mutant showing furrows ingressing between all nuclei, but no Arm accumulating at basal junctions. Truncated Arm instead accumulates apically (arrows). (D,E) TEM images showing furrows ingressing in cellularizing embryos. Arrows indicate the furrow shown at higher magnification in the right-hand images, and arrowheads indicate the position where the basal junctions should be. (D) In wild-type embryos, adjacent PMs are tightly apposed. (E) In *arm*[043A01] embryos, adjacent PMs gape apart. Furrow tips broaden into furrow canals despite the absence of basal junctions. (F,G) Confocal images of Myosin 2 furrow canals (Myo-2, green) in cellularizing embryos. (F) En face images from a single plane at the level of the furrow canals at progressive phases of cellularization showing that furrow canals form around all nuclei (Early) and later constrict (Late). (G) Cross-section of *arm*[043A01] mutant showing tear-shaped furrow canals that lack staining for a lateral PM probe (Nrt, red). (H) Cross-sections showing F-actin (phalloidin) in cellularizing embryos. Images collected at the same settings show no difference between F-actin levels for wild-type versus *arm*[043A01] embryos. (I) F-actin levels quantified in furrow canals of wild-type (black) versus *arm*[043A01] (red) embryos at progressive phases of cellularization, as measured by fluorescent intensity of phalloidin staining. Each point represents one embryo in which 75-100 furrow canals were analyzed. Error bars represent s.d. Scale bars: 5 μm in A-C,F-H and 2 μm in D,E.

mutant furrow canals (Fig. 5D), consistent with Nullo acting upstream of Anillin and Septin localization during cellularization. Similar to *nulloX* embryos, cross-sections clearly showed that all furrow canals take on a flat morphology in embryos from either *anillin*[HP/RS] or *anillin*[PQ/RS] mothers (Field, C. et al., 2005; Thomas and Wieschaus, 2004). Nonetheless, compartmentalization was unperturbed, with the lateral markers Dlg and Nrt accumulating in the lateral PM but not entering the furrow canals (Fig. 5B,C). In addition, neither Myosin 2 nor F-actin levels were compromised in furrow canals of the *anillin*-deficient embryos at early cellularization (data not shown; Fig. 5E,F; *n*=3 independent experiments). Thus, furrow compartmentalization appears to be independent of these particular cortical scaffolds.

Within the initial segment of the mammalian neuron, Ankyrin-G-dependent compartmentalization develops as F-actin accumulates in the underlying cortex (Nakada et al., 2003), and F-actin perturbation increases the mobility of lipids and proteins within the initial segment while promoting exchange of components that are normally restricted to either the cell body or axon (Nakada et al., 2003; Winckler et al., 1999). Thus, the cortical F-actin meshwork at the initial segment is crucial to establishing and maintaining this membrane compartment. We have shown that Nullo regulates cortical F-actin levels in cellularizing embryos: in *nulloX* embryos, F-actin levels are reduced to approximately half those in the wild type at every persisting furrow canal from the onset of cellularization (Sokac and Wieschaus, 2008). We wondered whether the reduction in F-actin levels in *nulloX* mutants could account for their failure to establish and/or maintain furrow canal compartments.

To determine whether reduced F-actin levels in *nulloX* embryos compromise furrow canal compartmentalization, we generically reduced F-actin levels with the F-actin-destabilizing drug Cytochalasin-D (Cyto-D). Wild-type embryos (OreR) were permeabilized, treated with Cyto-D, and the distribution of furrow markers determined. We chose a low dose of Cyto-D compared with that previously used in permeabilized embryos, with the intention of reducing but not completely disrupting F-actin (Harris and Peifer, 2005; Townsley and Bienz, 2000). Following treatment with low doses of Cyto-D, Myosin 2 and Anillin furrow canals were absent from some furrows (Fig. 6A-C,E). Some early furrows showed spreading of the lateral PM marker Dlg into the furrow canal compartment (Fig. 6C; furrow length <5 µm). In older embryos (furrow length >5 µm), Myosin 2 was missing from some furrows (Fig. 6A), and the lateral PM markers Dlg and Nrt spread into some furrow canals, suggesting that the PM compartments were not well maintained (Fig. 6D,E). En face images clearly showed that Cyto-D treatment precipitated both breaks in the Myosin 2 furrow canal network and regression of some furrows, and this phenotype was increasingly severe at higher doses of Cyto-D (Fig. 6A). These results are consistent with a role for cortical F-actin in compartmentalizing cellularization furrows. We also found that Nullo concentrates at furrow canals following Cyto-D treatment, suggesting that Nullo localizes independently of F-actin (Fig. 6H). Interestingly, we noted that the low dose of Cyto-D also disrupted basal junctions (Fig. 6F,G), as is seen in *nulloX* embryos (Hunter and Wieschaus, 2000). Thus, reducing F-actin levels generically with Cyto-D essentially mimics the cellularization defects observed in *nulloX* mutants. These data are consistent with a model whereby Nullo establishes and maintains furrow canal compartments via its regulation of F-actin.

Discussion

The establishment of compartments around the cortical F-actin/Myosin 2 array appears to be a conserved feature of furrowing during conventional cytokinesis, common from yeast (Dobbelaere and Barral, 2004; Takeda et al., 2004; Wachtler et al., 2003), to sea urchin and *Xenopus* embryos (Byers and Armstrong, 1986), to cultured mammalian cells (Schmidt and Nichols, 2004). Previous

Fig. 5. Furrow canal compartments are established and maintained in *anillin*-deficient embryos. (A-E) Confocal images of cellularizing embryos derived from *anillin*[HP/RS] or wild-type mothers. (A) En face images from a single plane, showing that Septin (green) fails to accumulate in furrow canals [Myosin 2 (Myo-2), red] of *anillin*-deficient mutants. (B) Cross-section of an *anillin*-deficient mutant showing that furrow canals (Myo-2, green) lack staining for a lateral PM probe (Dlg, red). (C) Cross-section of an *anillin*-deficient mutant showing that collapsed furrow canals (Myo-2, green) lack staining for a lateral PM probe (Nrt, red). (D) En face images from a single plane, showing that Nullo (green) accumulates normally in furrow canals of *anillin*-deficient mutants. (E) Cross-sections showing F-actin (phalloidin) in cellularizing embryos. Images collected at the same settings show no difference between F-actin levels for wild-type versus *anillin*-deficient embryos. (F) F-actin levels quantified in furrow canals of wild-type (black) versus *anillin*-deficient (red) embryos at progressive phases of cellularization, as measured by fluorescent intensity of phalloidin staining. Each point represents one embryo in which 75-100 furrow canals were analyzed. Error bars represent s.d. Scale bars: 5 µm.
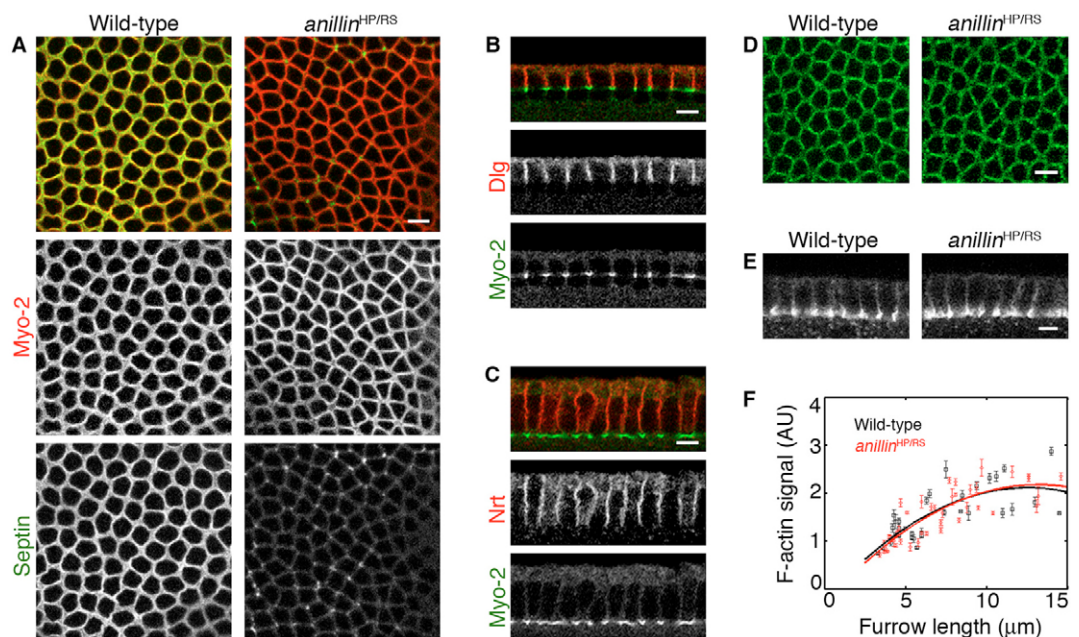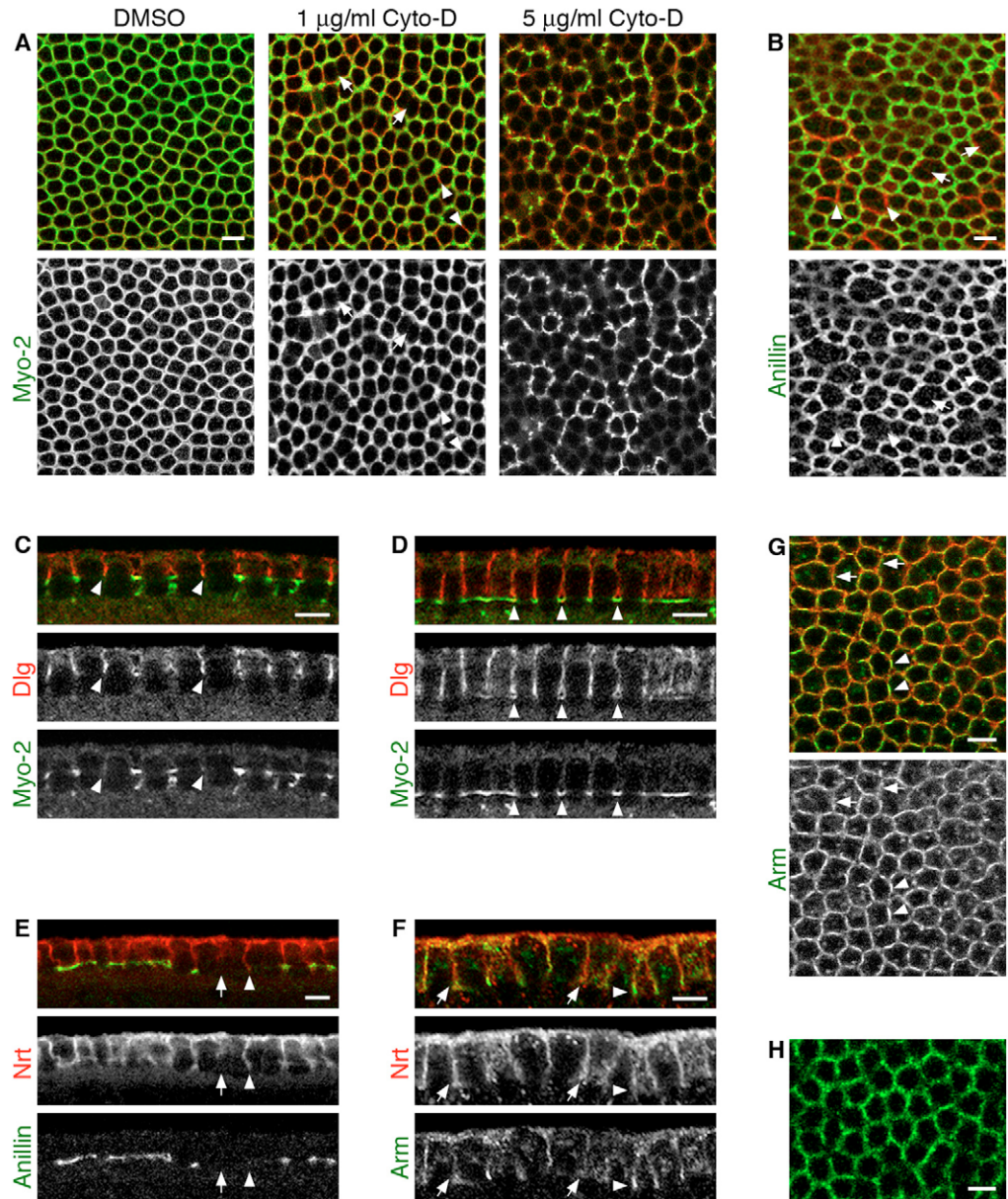
Fig. 6. F-actin disruption mimics *nulloX* phenotypes. (A-E) Confocal images of PM furrows ingressing between adjacent nuclei in cellularizing wild-type embryos treated with Cyto-D. (A) En face images collected in a single plane at the level of the furrow canals showing that in embryos treated with a low dose of Cyto-D, some furrows (Dlg, red) are missing (arrows) or have no Myosin 2 (Myo-2, green) in the furrow canals (arrowheads). The furrow canal network is severely disrupted in embryos treated with higher doses of Cyto-D. (B) En face image collected in a single plane at the level of the furrow canals showing that in embryos treated with 1 μg/ml Cyto-D, some furrows (Nrt, red) are missing (arrows) or have no Anillin (green) in the furrow canals (arrowheads). (C) Cross-section from an embryo treated with 1 μg/ml Cyto-D showing Myosin 2 furrow canals (green) are absent from some furrows (Dlg, red; arrowheads). (D) Cross-section from an embryo treated with 1 μg/ml Cyto-D showing Dlg (red) spreading into some Myosin 2 furrow canals (green; arrowheads). (E) Cross-section from an embryo treated with 1 μg/ml Cyto-D showing some furrows (Nrt, red) are missing between adjacent nuclei (arrow) or have no Anillin (green) in the furrow canals (arrowhead). (F,G) Confocal images of PM furrows (Nrt, red) and basal junctions (Arm, green) in cellularizing wild-type embryos treated with 1 μg/ml Cyto-D. (F) Cross-sections showing basal junction defects, ranging from furrows that have some basal Arm accumulation (arrowhead) to those that have none (arrows). (G) En face images from a single plane at the level of the basal junctions showing basal junction defects, ranging from Arm plaques at some furrows (arrowheads) to diffuse Arm puncta at others (arrows). (H) En face images from a single plane, showing that Nullo (green) accumulates normally in furrow canals of Cyto-D-treated embryos. Scale bars: 5 μm.

analyses in cellularizing *Drosophila* embryos similarly suggested that the F-actin/Myosin 2 furrow canals are discrete compartments that form at the tips of incipient furrows and are maintained as the furrows ingress (Lecuit and Wieschaus, 2000). According to the data we present here, compartmentalization of the cellularization furrow emerges as an essential cellular mechanism to concentrate cortical components at the furrow canal and so ensure sustained furrow ingression. We identify Nullo as a developmental regulator that aids compartment establishment and maintenance. Nullo activity serves to partition proteins along the furrow from the beginning of cellularization, retaining cortical components such as Myosin 2 at the furrow canal while excluding the lateral proteins Dlg and Nrt. In this way, Nullo stabilizes furrows such that they ingress to convert the syncytial embryo into a primary epithelial sheet.

Our data show that Nullo is unlikely to compartmentalize the cellularization furrow via basal junctions or the cortical scaffold proteins Anillin or Septin, and instead supports a model whereby Nullo regulates cortical F-actin to establish and then maintain furrow canal compartments. In *nulloX* embryos, furrow canal breaks and regression occur at only a fraction of furrows. This is in contrast to the global expression profile of Nullo protein. Discontinuous furrow canal phenotypes have similarly been reported following alternative perturbations of cortical F-actin in cellularizing embryos. For example, Cyto-B injection does not halt furrowing, but rather induces breaks in the Myosin 2 furrow canal network (Royou et al., 2004). *RhoGEF2* and *diaphanous* (*dia*) mutants, which also have reduced F-actin levels at furrow canals, are also missing some furrow canals (Grosshans et al., 2005; Padash Barmchi et al., 2005). Taken together, we now suggest that reduced F-actin compromises

furrow canal compartments at all furrows. In support of this, we find that furrow canal morphology is altered at all furrows and lateral PM components spread into every furrow canal in *nulloX* mutants. However, the spreading of lateral components is not sufficient to precipitate furrow regression. Instead, it is the stochastic loss of cortical components from the furrow canal that destabilizes furrows to the extreme that they may regress. In the case of *nulloX* embryos, we find that even in the absence of furrow canal components such as Myosin 2, as long as the furrow canal contains some F-actin, the associated furrow continues to ingress. But these furrows appear to be sensitized and perhaps the continued dilution of furrow canal actin by the spreading lateral PM components eventually precipitates their regression.

Several published results now suggest that, in addition to Nullo, the Rho1 GTPase may contribute to furrow compartmentalization. Rho1 and its activator, RhoGEF2, localize to furrow canals and the lateral furrow membrane during cellularization, suggesting that Rho1 is specifically activated there (Grosshans et al., 2005; Padash Barmchi et al., 2005). RhoGEF2 localization is independent of F-actin (Grosshans et al., 2005), and in *RhoGEF2* mutants Dia fails to accumulate at the furrow canal and the embryos have reduced levels of cortical F-actin (Padash Barmchi et al., 2005; Grosshans et al., 2005). Interestingly, *RhoGEF2* and *dia* mutants show phenotypes strikingly similar to *nulloX* mutants in that some furrow canals are missing (Grosshans et al., 2005; Padash Barmchi et al., 2005). This supports our assertion that cortical F-actin helps to maintain furrow canal integrity. Furthermore, following RNAi depletion of *nullo* in *RhoGEF2* mutants, F-actin does not assemble at furrow canals, and so the two proteins may function in separate but parallel pathways (Grosshans et al., 2005). We thus favor a model whereby the combined activities of Nullo and Rho1 provide the full complement of F-actin at and around the furrow canal, which is in turn required to establish and/or maintain the furrow canal compartment.

Why would reduced cortical F-actin compromise furrow compartmentalization? One possibility is that F-actin recruits and/or retains particular cytoskeletal or scaffold proteins at the furrow canal that are required for compartment establishment and/or maintenance. In fact, in *nulloX* and Cyto-D-treated embryos, Myosin 2, Anillin and Septin are missing from some furrow canal compartments. This mechanism is consistent with that of the axon initial segment, where PM compartments develop by the progressive recruitment of the scaffold protein Ankyrin G that tethers cortical F-actin/Spectrin to the PM (Dzhashiashvili et al., 2007; Nakada et al., 2003; Winckler et al., 1999). The resulting meshwork traps and concentrates additional proteins in the compartment, including transmembrane receptors and ion channels (Dzhashiashvili et al., 2007; Nakada et al., 2003). Alternatively, F-actin levels might control membrane trafficking events that occur at the furrow canal compartment. In support of this, we see cytoplasmic Myosin 2 punctae following F-actin perturbation in cellularizing embryos (data not shown), which might represent some form of trafficking intermediate. Since cortical F-actin modulates both endocytosis (Kaksonen et al., 2006) and exocytosis (Ehre et al., 2005; Valentijn et al., 1999), changes in actin level might change the rates of membrane and/or protein uptake and delivery within PM compartments (Gheber and Edidin, 1999; Marco et al., 2007). Lastly, F-actin levels at the furrow canal might promote lipid heterogeneities at the PM in the form of lipid micro-domains or rafts, as has been reported in a spectrum of mammalian cell types and in sea urchin embryos (Holowka et al., 2000; Oliferenko et al., 1999; Seveau et al., 2001; Wu et al., 2004).

Lipid rafts may then define compartments by virtue of their intrinsic chemical properties or by recruiting additional signaling or scaffolding complexes (Maxfield and Tabas, 2005). Of course, during cellularization these mechanisms may not be mutually exclusive, but should converge on the formation and maintenance of discrete furrow canal compartments that stabilize furrows and ensure their sustained ingression.

Materials and Methods

Flies and genetics
Germline clones for *arm^{043A01}* (Tolwinski and Wieschaus, 2001) were prepared by standard FLP-DFS techniques (Chou and Perrimon, 1992). The *anillin*-deficient embryos were prepared by crossing *anillin^{HP/RS}* or *anillin^{PQ/RS}* transheterozygous mothers with *anillin^{HP}* or *anillin^{PQ}* heterozygous fathers, respectively (Schupbach and Wieschaus, 1989). The *nulloX* (X) embryos were collected from the C(1)DX, *ywf* stock (Wieschaus and Sweeton, 1988). The cellularization phenotypes of these *nulloX* embryos were rescued with a *nullo* transgene (Hunter et al., 2002; Rose and Wieschaus, 1992). For live imaging, the stock C(1)DX, *ywf*; Spider-GFP was prepared by making the insertion *95-1 spider-GFP* (III; Gavdos Protein Trap, Observatoire Océanologique, Villefranche-sur-mer, France) homozygous in C(1)DX, *ywf*. For Nullo colocalization with F-actin, ectopic *nullo-HA* embryos were generated by crossing males homozygous for *UASnullo-HA3A* (III; hop of insertion *N39*) (Hunter and Wieschaus, 2000) with females homozygous for *matα4-GAL-VP16* (II and III). Fixed embryos were genotyped by absence of Sex lethal (Sxl) or Arm expression (*arm^{043A01}*), reduced Anillin expression or Septin mislocalization (*anillin* deficient), or by absence of Runt expression (*nulloX*).

Permeabilization, fixation and antibody staining
For drug treatment embryos were permeabilized (Townsley and Bienz, 2000), incubated for 10 minutes in 1-5 µg/ml Cyto-D (Calbiochem; reconstituted in either DMSO or 100% ethanol) and immediately fixed (see below).

For immunofluorescence, embryos were fixed in boiling salt buffer (Muller and Wieschaus, 1996) and vitelline membranes removed by methanol:heptane (1:1) for staining with the following antibodies: mouse anti-Nullo (1:5); rabbit anti-Myosin 2 (1:1400, gift of C. Field, Harvard University, Boston, MA), mouse anti-Nrt (1:100, BP106, Developmental Studies Hybridoma Bank (DSHB)], mouse anti-Arm (1:50, N2-7A1, DSHB), rabbit anti-Arm (1:50), rat anti-HA (1:50, Roche) and guinea pig anti-Runt (1:500, gift of J. Reinitz, Stony Brook University, NY). Embryos were fixed for 20 minutes in 4% formaldehyde/0.1 M phosphate buffer (pH 7.4):heptane (1:1), and vitelline membranes removed by methanol:heptane for staining with the following antibodies: rabbit anti-Myosin 2 (1:1000), rabbit anti-Anillin (1:1000, gift of C. Field), rat anti-E-cadherin (1:50, DCAD2, DSHB), mouse anti-Septin (1:5, 4C9H4, DSHB) and mouse anti-Sxl (1:10, M-14, DSHB). Embryos were fixed for 30 minutes in 18.5% formaldehyde/0.1 M phosphate buffer (pH 7.4):heptane (1:1), and vitelline membranes removed by hand for staining with Alexa488-phalloidin (5U/ml, Molecular Probes). For detections, goat secondary antibodies were Alexa488-, Alexa546-, or Alexa647-conjugated (1:500, Molecular Probes). DNA was stained with Hoescht 33342 (1 µg/ml, Molecular Probes). Embryos were mounted in AquaPolymount (Polysciences). Confocal images were collected on a Zeiss LSM 510 microscope (Carl Zeiss, Thornwood, NY) with a numerical aperture 1.2, 40× objective lens.

For TEM, embryos were fixed according to McDonald, Sharp and Rickoll (Sullivan et al., 2000). Unstained 70 nm sections were cut with a diamond knife on a Leica UC6 ultramicrotome (Leica Microsystems, Bannockburn, IL). Electron micrographs were collected at 80 kV on a Zeiss 912AB transmission electron microscope equipped with an Omega Energy Filter (Carl Zeiss).

Live imaging
For furrow ingression analysis, embryos were mounted in halocarbon oil 27 (Sigma-Aldrich) and confocal images collected on a Nikon Eclipse E800 microscope (Nikon, Melville, NY)/CARV non-laser spinning disc system (BD Biosciences, Houston, TX) with a numerical aperture 1.3, 60× objective.

Image analysis and quantification
For quantification of F-actin fluorescence intensity in furrow canals, three 12-bit confocal cross-sections were collected at the dorsal equator for each embryo. Within a given experiment, all laser settings were constant. In MATLAB (Image Processing Toolbox, The MathWorks, Natick, MA) all furrow canals in an image were identified by thresholding and then hand-selected to eliminate falsely identified objects (to verify the technique, we tested a range of threshold values, all giving the same trend). Mean fluorescent intensity and standard error were calculated per image. Mean intensities from the three images were averaged and standard deviation calculated such that each data point on the plot represents ~100 furrow canals from one embryo. Data were plotted using MATLAB and curves fitted to a second-order polynomial.

For quantification of *nulloX* furrow types, *z*-sections were projected from confocal image stacks with Volocity software (Improvision, Lexington, MD) along the *x*-axis at every 50-pixel interval along the *y*-axis. From any given embryo ~200 furrows

References

Albertson, R., Riggs, B. and Sullivan, W. (2005). Membrane traffic: a driving force in cytokinesis. *Trends Cell Biol.* **15**, 92-101.

Byers, T. J. and Armstrong, P. B. (1986). Membrane protein redistribution during Xenopus first cleavage. *J. Cell Biol.* **102**, 2176-2184.

Chou, T. B. and Perrimon, N. (1992). Use of a yeast site-specific recombinase to produce female germline chimeras in Drosophila. *Genetics* **131**, 643-653.

Cox, R. T., Kirkpatrick, C. and Peifer, M. (1996). Armadillo is required for adherens junction assembly, cell polarity, and morphogenesis during Drosophila embryogenesis. *J. Cell Biol.* **134**, 133-148.

Dawes-Hoang, R. E., Parmar, K. M., Christiansen, A. E., Phelps, C. B., Brand, A. H. and Wieschaus, E. F. (2005). Folded gastrulation, cell shape change and the control of myosin localization. *Development* **132**, 4165-4178.

De Renzis, S., Elemento, O., Tavazoie, S. and Wieschaus, E. F. (2007). Unmasking activation of the zygotic genome using chromosomal deletions in the Drosophila embryo. *PLoS Biol.* **5**, e117.

Dobbelaere, J. and Barral, Y. (2004). Spatial coordination of cytokinetic events by compartmentalization of the cell cortex. *Science* **305**, 393-396.

Dzhashiashvili, Y., Zhang, Y., Galinska, J., Lam, I., Grumet, M. and Salzer, J. L. (2007). Nodes of Ranvier and axon initial segments are ankyrin G-dependent domains that assemble by distinct mechanisms. *J. Cell Biol.* **177**, 857-870.

Ehre, C., Rossi, A. H., Abdullah, L. H., De Pestel, K., Hill, S., Olsen, J. C. and Davis, C. W. (2005). Barrier role of actin filaments in regulated mucin secretion from airway goblet cells. *Am. J. Physiol. Cell Physiol.* **288**, C46-C56.

Field, C. M. and Alberts, B. M. (1995). Anillin, a contractile ring protein that cycles from the nucleus to the cell cortex. *J. Cell Biol.* **131**, 165-178.

Field, C. M., Coughlin, M., Doberstein, S., Marty, T. and Sullivan, W. (2005). Characterization of anillin mutants reveals essential roles in septin localization and plasma membrane integrity. *Development* **132**, 2849-2860.

Field, S. J., Madson, N., Kerr, M. L., Galbraith, K. A., Kennedy, C. E., Tahiliani, M., Wilkins, A. and Cantley, L. C. (2005). PtdIns(4,5)P2 functions at the cleavage furrow during cytokinesis. *Curr. Biol.* **15**, 1407-1412.

Gheber, L. A. and Edidin, M. (1999). A model for membrane patchiness: lateral diffusion in the presence of barriers and vesicle traffic. *Biophys. J.* **77**, 3163-3175.

Grevengoed, E. E., Fox, D. T., Gates, J. and Peifer, M. (2003). Balancing different types of actin polymerization at distinct sites: roles for Abelson kinase and Enabled. *J. Cell Biol.* **163**, 1267-1279.

Grosshans, J., Wenzl, C., Herz, H. M., Bartoszewski, S., Schnorrer, F., Vogt, N., Schwarz, H. and Muller, H. A. (2005). RhoGEF2 and the formin Dia control the formation of the furrow canal by directed actin assembly during Drosophila cellularization. *Development* **132**, 1009-1020.

Harris, T. J. and Peifer, M. (2004). Adherens junction-dependent and -independent steps in the establishment of epithelial cell polarity in Drosophila. *J. Cell Biol.* **167**, 135-147.

Harris, T. J. and Peifer, M. (2005). The positioning and segregation of apical cues during epithelial polarity establishment in Drosophila. *J. Cell Biol.* **170**, 813-823.

Holowka, D., Sheets, E. D. and Baird, B. (2000). Interactions between Fc(epsilon)RI and lipid raft components are regulated by the actin cytoskeleton. *J. Cell Sci.* **113**, 1009-1019.

Hunter, C. and Wieschaus, E. (2000). Regulated expression of nullo is required for the formation of distinct apical and basal adherens junctions in the Drosophila blastoderm. *J. Cell Biol.* **150**, 391-401.

Hunter, C., Sung, P., Schejter, E. D. and Wieschaus, E. (2002). Conserved domains of the Nullo protein required for cell-surface localization and formation of adherens junctions. *Mol. Biol. Cell* **13**, 146-157.

Kaksonen, M., Toret, C. P. and Drubin, D. G. (2006). Harnessing actin dynamics for clathrin-mediated endocytosis. *Nat. Rev. Mol. Cell Biol.* **7**, 404-414.

Lecuit, T. and Wieschaus, E. (2000). Polarized insertion of new membrane from a cytoplasmic reservoir during cleavage of the Drosophila embryo. *J. Cell Biol.* **150**, 849-860.

Lee, O. K., Frese, K. K., James, J. S., Chadda, D., Chen, Z. H., Javier, R. T. and Cho, K. O. (2003). Discs-Large and Strabismus are functionally linked to plasma membrane formation. *Nat. Cell Biol.* **5**, 987-993.

Marco, E., Wedlich-Soldner, R., Li, R., Altschuler, S. J. and Wu, L. F. (2007). Endocytosis optimizes the dynamic localization of membrane proteins that regulate cortical polarity. *Cell* **129**, 411-422.

Maxfield, F. R. and Tabas, I. (2005). Role of cholesterol and lipid organization in disease. *Nature* **438**, 612-621.

Mazumdar, A. and Mazumdar, M. (2002). How one becomes many: blastoderm cellularization in Drosophila melanogaster. *BioEssays* **24**, 1012-1022.

Muller, H. A. and Wieschaus, E. (1996). armadillo, bazooka, and stardust are critical for early stages in formation of the zonula adherens and maintenance of the polarized blastoderm epithelium in Drosophila. *J. Cell Biol.* **134**, 149-163.

Nakada, C., Ritchie, K., Oba, Y., Nakamura, M., Hotta, Y., Iino, R., Kasai, R. S., Yamaguchi, K., Fujiwara, T. and Kusumi, A. (2003). Accumulation of anchored proteins forms membrane diffusion barriers during neuronal polarization. *Nat. Cell Biol.* **5**, 626-632.

Oliferenko, S., Paiha, K., Harder, T., Gerke, V., Schwarzler, C., Schwarz, H., Beug, H., Gunthert, U. and Huber, L. A. (1999). Analysis of CD44-containing lipid rafts: Recruitment of annexin II and stabilization by the actin cytoskeleton. *J. Cell Biol.* **146**, 843-854.

Padash Barmchi, M., Rogers, S. and Hacker, U. (2005). DRhoGEF2 regulates actin organization and contractility in the Drosophila blastoderm embryo. *J. Cell Biol.* **168**, 575-585.

Peifer, M. and Wieschaus, E. (1990). The segment polarity gene armadillo encodes a functionally modular protein that is the Drosophila homolog of human plakoglobin. *Cell* **63**, 1167-1176.

Pesacreta, T. C., Byers, T. J., Dubreuil, R., Kiehart, D. P. and Branton, D. (1989). Drosophila spectrin: the membrane skeleton during embryogenesis. *J. Cell Biol.* **108**, 1697-1709.

Postner, M. A. and Wieschaus, E. F. (1994). The nullo protein is a component of the actin-myosin network that mediates cellularization in Drosophila melanogaster embryos. *J. Cell Sci.* **107**, 1863-1873.

Rose, L. S. and Wieschaus, E. (1992). The Drosophila cellularization gene nullo produces a blastoderm-specific transcript whose levels respond to the nucleocytoplasmic ratio. *Genes Dev.* **6**, 1255-1268.

Royou, A., Field, C., Sisson, J. C., Sullivan, W. and Karess, R. (2004). Reassessing the role and dynamics of nonmuscle myosin II during furrow formation in early Drosophila embryos. *Mol. Biol. Cell* **15**, 838-850.

Schejter, E. D. and Wieschaus, E. (1993). Functional elements of the cytoskeleton in the early Drosophila embryo. *Annu. Rev. Cell Biol.* **9**, 67-99.

Schmidt, K. and Nichols, B. J. (2004). A barrier to lateral diffusion in the cleavage furrow of dividing mammalian cells. *Curr. Biol.* **14**, 1002-1006.

Schupbach, T. and Wieschaus, E. (1989). Female sterile mutations on the second chromosome of Drosophila melanogaster. I. Maternal effect mutations. *Genetics* **121**, 101-117.

Seveau, S., Eddy, R. J., Maxfield, F. R. and Pierini, L. M. (2001). Cytoskeleton-dependent membrane domain segregation during neutrophil polarization. *Mol. Biol. Cell* **12**, 3550-3562.

Shapiro, L., Fannon, A. M., Kwong, P. D., Thompson, A., Lehmann, M. S., Grubel, G., Legrand, J. F., Als-Nielsen, J., Colman, D. R. and Hendrickson, W. A. (1995). Structural basis of cell-cell adhesion by cadherins. *Nature* **374**, 327-337.

Sokac, A. M. and Wieschaus, E. (2008). Local actin-dependent endocytosis is zygotically controlled to initiate Drosophila cellularization. *Dev. Cell* (in press).

Sullivan, W., Ashburner, M. and Hawley, R. S. (ed.) (2000). *Drosophila Protocols*. Cold Spring Harbor, NY: Cold Spring Harbor Laboratory Press.

Takeda, T., Kawate, T. and Chang, F. (2004). Organization of a sterol-rich membrane domain by cdc15p during cytokinesis in fission yeast. *Nat. Cell Biol.* **6**, 1142-1144.

Thomas, G. H. and Williams, J. A. (1999). Dynamic rearrangement of the spectrin membrane skeleton during the generation of epithelial polarity in Drosophila. *J. Cell Sci.* **112**, 2843-2852.

Thomas, J. H. and Wieschaus, E. (2004). src64 and tec29 are required for microfilament contraction during Drosophila cellularization. *Development* **131**, 863-871.

Tolwinski, N. S. and Wieschaus, E. (2001). Armadillo nuclear import is regulated by cytoplasmic anchor Axin and nuclear anchor dTCF/Pan. *Development* **128**, 2107-2117.

Townsley, F. M. and Bienz, M. (2000). Actin-dependent membrane association of a Drosophila epithelial APC protein and its effect on junctional Armadillo. *Curr. Biol.* **10**, 1339-1348.

Valentijn, K. M., Gumkowski, F. D. and Jamieson, J. D. (1999). The subapical actin cytoskeleton regulates secretion and membrane retrieval in pancreatic acinar cells. *J. Cell Sci.* **112**, 81-96.

Wachtler, V., Rajagopalan, S. and Balasubramanian, M. K. (2003). Sterol-rich plasma membrane domains in the fission yeast Schizosaccharomyces pombe. *J. Cell Sci.* **116**, 867-874.

Warn, R. M. and Magrath, R. (1983). F-actin distribution during the cellularization of the Drosophila embryo visualized with FL-phalloidin. *Exp. Cell Res.* **143**, 103-114.

Warn, R. M., Bullard, B. and Magrath, R. (1980). Changes in the distribution of cortical myosin during the cellularization of the Drosophila embryo. *J. Embryol. Exp. Morphol.* **57**, 167-176.

Wieschaus, E. (1996). Embryonic transcription and the control of developmental pathways. *Genetics* **142**, 5-10.

Wieschaus, E. and Sweeton, D. (1988). Requirements for X-linked zygotic gene activity during cellularization of early Drosophila embryos. *Development* **104**, 483-493.

Winckler, B. and Mellman, I. (1999). Neuronal polarity: controlling the sorting and diffusion of membrane components. *Neuron* **23**, 637-640.

Winckler, B., Forscher, P. and Mellman, I. (1999). A diffusion barrier maintains distribution of membrane proteins in polarized neurons. *Nature* **397**, 698-701.

Wu, M., Holowka, D., Craighead, H. G. and Baird, B. (2004). Visualization of plasma membrane compartmentalization with patterned lipid bilayers. *Proc. Natl. Acad. Sci. USA* **101**, 13798-13803.